Greenhouse gas emissions from a Siberian alas ecosystem near Yakutsk, Russia

Fumiaki Takakai[1,*], Alexey R. Desyatkin[2], Larry Lopez[3], Ryusuke Hatano[1,4],
Alexander N. Fedorov[5], and Roman V. Desyatkin[2]

[1]*Graduate School of Agriculture, Hokkaido University, Kita-9 Nishi-9, Kita-ku, Sapporo 060-8589, Japan*
[2]*Institute for Biological Problems of Cryolithozone, Siberian Branch, Russian Academy of Science, Lenin Ave. 41, Yakutsk 677980, Russia*
[3]*Institute of Low Temperature Science, Hokkaido University, Kita-19 Nishi-8, Kita-ku, Sapporo 060-0819, Japan*
[4]*Field Science Center for Northern Biosphere, Hokkaido University, Kita-9 Nishi-9, Kita-ku, Sapporo 060-8589, Japan*
[5]*Permafrost Institute, SB RAS, Yakutsk 6770010, Russia*

[*]*Corresponding author: takakai@chem.agr.hokudai.ac.jp*

1. INTRODUCTION

Many natural wetlands take up CO_2 and accumulate its carbon as peat (Clymo 1984). Northern wetlands contain about one-third (455 Pg C) of the total world pool of soil carbon (Gorham 1991). Recently, the long-term apparent rate of carbon accumulation (LORCA) was estimated in various boreal wetlands. To estimate LORCA, researchers have divided the accumulated mass of carbon above the peat–mineral contact by the age of the basal peat based on ^{14}C dating. The results of this LORCA analysis for boreal peatlands vary according to the wetland type, with average values ranging from 15 to 35 g C m^{-2} yr^{-1} (Botch et al. 1995, Turunen et al. 2002). Thus, natural wetland ecosystems act as a carbon sink on a long-term basis. On the other hand, the short-term carbon balance of natural wetlands measured using a closed-chamber method and an eddy-covariance method revealed results ranging from net uptake to net release. The interannual differences in carbon balance appear to have been caused mainly by simultaneous variations in climate (Aurela et al. 2004; Waddington and Roulet, 2000). In addition, differences in the carbon balance of various microsites were caused by spatial variation in the water regime, vegetation, microtopography, and other factors (Heikkinen et al. 2002).

In addition to sequestering carbon, natural wetlands produce and emit methane (CH_4) as a result of anaerobic decomposition of organic matter. CH_4 is the second-most important greenhouse gas next to CO_2, and contributes an estimated 20% of the radiative forcing of the global climate (IPCC 2001). Natural wetland ecosystems are one of the most important sources of CH_4. The global CH_4 emission from natural wetlands is estimated to be 92 Tg CH_4 yr^{-1} (Cao et al. 1998) to 111 Tg CH_4 yr^{-1} (Matthews and Fung 1987), and this accounted for about 20% of the total global source of CH_4 (598 Tg CH_4 yr^{-1}, IPCC 2001). Measurements of CH_4 emissions from natural wetlands were conducted mainly in the boreal region and were reported to exhibit high temporal and spatial variation. In many cases, the observed spatial variations in CH_4 emissions from wetlands were explained by changes in water table depth, soil temperature, and air pressure (e.g., Shurpali et al. 1993). Spatial variations in CH_4 emissions were also explained by differences in wetland type, water table depth, vegetation type, net ecosystem production (NEP), and other factors (e.g., Liblik and Moore 1997, Bellsario et al. 1999).

Symptom of Environmental Change in Siberian Permafrost Region,
Eds. Hatano R and Guggenberger G, p 11-25, Hokkaido University Press, Sapporo, 2006

Nitrous oxide (N_2O) is also an important greenhouse gas, but there have been fewer measurements of the N_2O flux from natural wetlands. At least one study suggests that peatlands could be an important source of N_2O as well as CO_2 after drying (Kasimir-Klemedtsson et al. 1997). However, N_2O emission from waterlogged peatlands was estimated to be small, and sometimes net N_2O uptake has been found. N_2O fluxes are reported to range from -0.7 to 5.3 μg N m^{-2} hr^{-1} (in a minerotrophic fen) and from -0.8 to 0.6 μg N m^{-2} hr^{-1} (in an ombrotrophic bog) in natural wetlands in eastern and central Finland (Regina et al. 1996).

The boreal taiga forest ecosystem has been considered to play an important role in the global carbon cycle because it serves as a huge carbon reservoir (Kolchugina and Vinson 1993). The Taiga forest around Yakutsk is characterized by the presence of permafrost (Desyatkin 1993) and occasional forest fires that burn large areas as a result of the area's low precipitation (Takahashi et al. 2003). There are many round areas of grassland that contain one or more ponds and that are called “alas” in taiga forest of central Yakutia. These ecosystems develop after damage to an area's forest ecosystem. Once the forest ecosystem growing in permafrost areas is severely damaged (e.g., because of forest fire or human activity), ice wedges within the permafrost start to melt. The increased water supply that results from melting of this ice and subsequent subsidence of the land surface lead to the formation of thermokarst ponds. Grassland areas then form as each pond begins drying up because evapotranspiration is higher than precipitation in this environment. This sequence requires more than 1000 years (Desyatkin 1993; Isaev 2001). The sizes of alas ecosystems vary from several tens of meters to several kilometers.

In general, forest ecosystems are considered to be significant CO_2 and CH_4 sinks, but they are slight sources for N_2O. The greenhouse gas (GHG) balance is believed to change as the forest ecosystem changes to an alas ecosystem. For example, Morishita et al. (2003) reported that the area around an alas pond became a strong source of CH_4 based on the flux measurements conducted during the summer.

To provide a clearer picture of the consequences of this ecosystem change, we measured all three GHGs (CO_2, CH_4, and N_2O) in the forest–alas ecosystem near Yakutsk, Russia. The purposes of this study were to (1) understand the seasonal changes in GHG fluxes, (2) quantify GHG emissions during the growing season, and (3) investigate the effect of alas formation on GHG emissions.

2. MATERIALS AND METHODS

2.1 Site description

The study site is the Neleger forest–alas ecosystem (62˚19’N, 129˚30’E) near Yakutsk, East Siberia, Russia. The alas at our study site is about 500 m wide (east to west) by 800 m long (north to south), with a roughly circular pond 100 m in diameter and 1 m deep at the center. Wet grassland was distributed around the pond, and dry grassland was distributed between the surrounding forest and the wet grassland. The pond area reaches its maximum in spring owing to the inflow of snowmelt water from the surrounding grassland and forest. However, the amount of evapotranspiration exceeds the amount of precipitation during the summer, leading to reduced water levels in the pond and a decrease in pond area.

The average annual temperature and precipitation for this region are -10 ˚C and 230 mm, respectively. The soil textural classes of the forest and the alas grassland are a silty clay loam and a silty clay, respectively. Detailed information on the alas and soil in the present study is provided by Morishita et al. (2003). The maximum thawing depths of the permafrost were about 1.0 m in forest plots and about 1.5 m in the alas grasslands. The accumulated masses of soil carbon above a depth of 30 cm were estimated to be 83.4, 11.8, and 16.4 to 30.8 Mg C ha^{-1}

for the forest, dry grassland, and wet grassland plots, respectively.

We established six plots on a line transect corresponding to the vegetation change from the adjoining forest to the alas pond (Fig. 1). The forest (F) consists mainly of 200-year-old larch (*Larix gmelinii*), with *Vaccinium vitis-idaea* on the forest floor. Dry grasslands (DG-1 and DG-2) were mainly dominated by *Elytrigia repens*. Wet grasslands (WG-1 and WG-2, the grasslands temporarily flooded by pond water) were dominated by several species of vascular plants (e.g., *Carex orthostachys*, *Glyceria lithuanica*). We defined the area with no vegetation that remained continuously flooded as the pond surface (P).

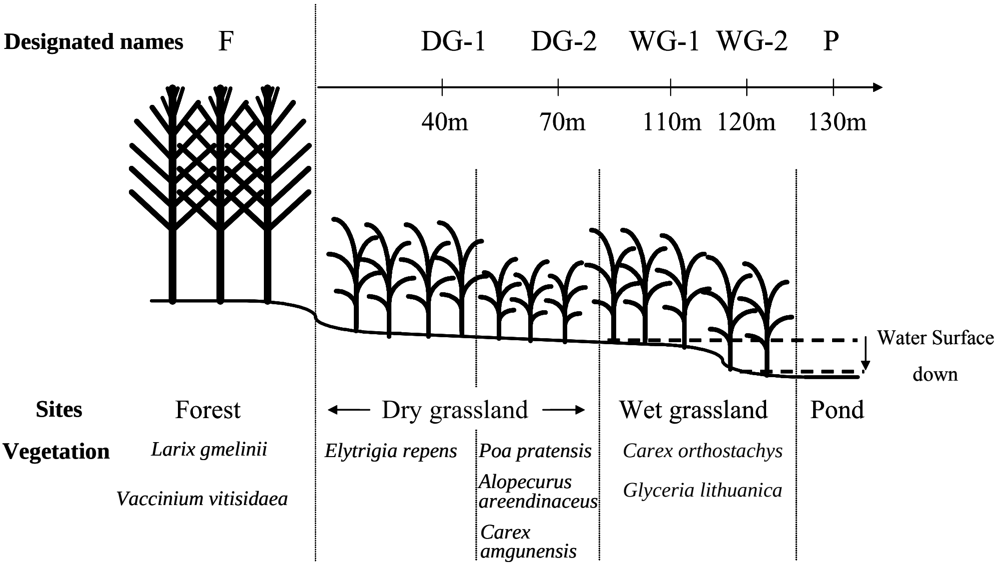

Fig. 1. Description of the transect in the Neleger alas study area.

2.2 Environmental variables

To evaluate the soil moisture regime along the line transect, we measured soil moisture (0 to 6 cm) six times, from the middle of June to the end of September, in 2004. We established the measurement sites in the forest plot and starting at the forest edge, then at 10-m intervals to a total distance of 120 to 130 m from the forest edge (i.e., at the edge of the pond). We monitored soil temperature at a depth of 3 cm at 1-h intervals using temperature dataloggers (TR-51, T & D, Japan) installed in the four grassland plots (DG-1, DG-2, WG-1, and WG-2). We monitored photosynthetically active radiation (PAR) at a height of 1.2 m using a PAR sensor (PAR-01, PREDE, Japan) at 10-min intervals and recorded the results using a datalogger (F80, MCS, Japan) in an open space adjacent to the alas. We interpolated gaps in the time series using data from a flux tower established in the larch forest (Machimura et al. 2005).

2.3 Measurement of GHG gas fluxes

We measured GHG fluxes two to three times per month using a closed-chamber method from June to September (108 days for F, DG-1, DG-2, WG-1, and WG-2, and 96 days for P). These measurements used two types of chamber (cylindrical stainless-steel chamber and open-bottomed rectangular transparent acryl chamber). Each stainless-steel chamber consisted of a stainless-steel cylinder and a detachable circular opaque lid. Each lid contained a gas-sampling tube, an inflatable plastic bag to control air pressure inside the chamber. To transport the chambers more conveniently to the field, we constructed the chambers so as to allow six chambers of slightly differing sizes to fit within each other (Morishita et al. 2003). That is, the height of each chamber was similar (25 cm), but the diameter differed (18.5, 19, 19.5, 20, 20.5, and 21 cm). We used the stainless-steel chambers for measurement of GHG from the soil surface. Vegetation inside the chamber was cut at ground level and removed and the chambers were installed to a depth of 3 cm below the soil surface one day before the measurements. We chose a different location for each measurement in the grassland plots to avoid the changes in soil moisture and temperature at clear cut place. We used the transparent acryl chambers (30 × 30 × 60 cm) for measurements in the plots dominated by grasses (from DG-1 to WG-2, four plots). During these measurements, we retained all plants inside the chamber so we could measure CO_2 uptake by photosynthesis, CO_2 emission from plant respiration, and CH_4 emission via the plants. Each chamber contained a gas-sampling tube, an inflatable plastic bag to control air pressure inside the chamber, and a thermistor thermometer to measure the air temperature inside the chamber. We inserted chamber collars (30 × 30 × 10 cm) equipped with a groove on the top into the soil to a depth of 5 cm in June 2004. We filled the groove with water and inserted the chamber into the groove during gas flux measurements. We used three replications for each measurement. For measurements using the transparent chambers, we recorded the air temperature inside each chamber during each gas sampling to assist in the calculation of gas fluxes. For measurements using the stainless-steel chambers, we recorded air temperatures outside the chamber for the same purpose. We measured soil temperature (during flooding, the water temperature) at a depth of 3 cm and volumetric soil water content from 0 to 6 cm in depth (using an ADR, DIK-311A, Daiki-rika, Japan) at the time of gas sampling. We also measured water depth at the time of gas sampling when the soil surface was flooded.

2.3.1 Measurement of CO_2 fluxes from soil and water surfaces (soil respiration)

We measured soil respiration using the stainless-steel chambers in all six plots. When the soil surface was flooded by pond water, we measured gas emissions from the water surface. At 0 and 6 min after closing the chamber with a lid, we collected a 500-mL gas sample in a 1-L Sampling bag (Tedlar® bag) using a 50-mL polypropylene syringe. We then analyzed the CO_2 concentration in the gas samples at our base camp adjacent to the Neleger alas site within the same day the sampling took place as described in section 2.4.

2.3.2 Measurement of CO_2 flux from the ecosystem

We measured net ecosystem exchange (NEE) of CO_2 using the transparent acryl chambers in four plots dominated by grasses (DG-1 to WG-2; Fig. 1). Details of the calculation procedure for NEE are presented in section 2.5 of this report. At 0 and 10 min after the chamber was inserted in the collar and closed, we collected a 500-mL gas sample in the same way described previously for the soil respiration measurements. In addition to soil temperature and moisture, we measured PAR as described above at the time of the gas sampling. In order to establish relationships between PAR and NEE at each sampling time, we covered the chambers with shading covers that provided two different levels of shading (50% and 100%) and measured NEE. The NEE of the completely darkened chamber (100% shading) was considered to present total ecosystem respiration in the absence of photosynthetic CO_2 uptake.

2.3.3 Measurement of CH_4 and N_2O fluxes

We measured CH_4 and N_2O fluxes from the soil surface using the stainless-steel chambers after each soil respiration measurement. We opened each chamber for more than 10 min after finishing the soil respiration measurement in order to completely exchange the air inside the chamber. At 0, 30, and 60 min after closing the top of the chamber with a lid, we collected a

20-mL gas sample in a 10-mL glass vacuum vial using a 25-mL polypropylene syringe. We returned these sample bottles to the laboratory of Hokkaido University (Sapporo, Japan) for analysis as described in section 2.4.

We measured whole-ecosystem CH_4 and N_2O fluxes (plant and soil) using the transparent acryl chambers in the four plots dominated by grasses (DG-1 to WG-2; Fig. 1). At 0, 10, and 20 min after inserting the chamber in the collar and closing its top, we collected a 20-mL gas sample in a 10-mL glass vacuum vial in the same way described previously for the stainless-steel chamber measurements.

2.4 Analysis of gas concentrations and flux calculations

We analyzed CO_2 concentrations with an infrared CO_2 analyzer (ZFP9, Fuji Electric Co., Ltd., Tokyo, Japan). We analyzed CH_4 and N_2O concentrations using gas chromatography (Shimadzu GC-8A and GC-14B, respectively) equipped with a flame ionization detector and an electron capture detector, respectively. We calculated the gas fluxes as follows:

$$F = \rho\times(V/A)\times(\Delta c/\Delta t)\times[273/(273+T)]\times\alpha \qquad (1)$$

where F is the flux (mg C m^{-2} hr^{-1} for CO_2, μg C m^{-2} hr^{-1} for CH_4 and μg Nm^{-2} hr^{-1} for N_2O), ρ is the gas density ($CO_2 = 1.98 \times 10^6$ mg m^{-3}, $CH_4 = 0.716 \times 10^9$ μg m^{-3}, $N_2O = 1.978 \times 10^9$ μg m^{-3}), V is the volume of the chamber (m^3), A is the cross-sectional area of the chamber (m^2), $\Delta c/\Delta t$ is the change in gas concentration inside the chamber during the sampling period (m^3 m^{-3} hr^{-1}), T is the air temperature inside the chamber (°C), and α is the conversion factor to transform CO_2 and CH_4 into C and N_2O into N (CO_2 = 12/44, CH_4 = 12/16, N_2O = 28/44). The minimum detectable concentrations of CO_2, CH_4, and N_2O were ±1.0, ±0.1, and ±0.01 ppmv, respectively. We calculated CO_2 fluxes by linear regression of two samples (at 0 and 6 min for the stainless-steel chambers and at 0 and 10 min for the transparent acryl chambers). We calculated CH_4 and N_2O fluxes by linear regression of three samples (at 0, 10, and 20 min for the transparent chambers and at 0, 30, and 60 min for the stainless-steel chambers).

2.5 Estimation of cumulative GHG flux

2.5.1 NEE of the grassland ecosystem

We calculated the cumulative NEE of the four grassland plots (DG-1 to WG-2; Fig. 1) using the method of Heikkinen et al. (2002). CO_2 fluxes from the whole ecosystem (plant and soil) consisted of emissions from the soil surface, photosynthetic uptake, and plant respiration. We used the transparent acryl chambers to determine NEE of CO_2 using the following equation:

$$NEE = R_{TOT} - P_G \qquad (2),$$

where R_{TOT} is the total ecosystem respiration in the completely darkened chambers, including respiration by soil organisms and plants, and P_G is the gross CO_2 uptake by photosynthesis. In terms of NEE, CO_2 uptake is a negative value and CO_2 emission to the atmosphere is a positive value. In the equation, both P_G and R_{TOT} are presented by absolute values.

According to equation (2), instantaneous gross photosynthesis (P_G) can be calculated by subtracting the NEE from R_{TOT}.

We constructed models using continuous PAR and soil temperature data to calculate the hourly rates of gross photosynthesis (P_G, equation 3) and total ecosystem respiration (R_{TOT}, equation 4):

$$P_G = (Q \times PAR) / (K+PAR) \qquad (3), \text{ and}$$
$$R_{TOT} = a \times e^{b \times T3cm} \qquad (4),$$

where Q is an asymptote at the maximum P_G, K is the light intensity at which 50% of the maximum P_G is reached, a and b are regression constants, and T3cm is the soil temperature at a depth of 3 cm. Equation (3) is a rectangular hyperbola for the relationship between P_G and PAR calculated using nonlinear regression in the Kaleidagraph 3.6J software (Synergy Software, USA). In equation (4), the total ecosystem respiration has an exponential dependence on soil temperature.

We calculated hourly P_G and R_{TOT} values from equations (3) and (4), then calculated hourly NEE using Equation (2). The cumulative NEE (for 109 days, from 13 June to 30 September) equals the sum of the hourly NEE values.

2.5.2 NEE of other ecosystems

We used the NEE value for the forest plot (F) that was calculated in a previous study (Sawamoto et al. 2003) to permit a comparison with values for other ecosystems. Sawamoto et al. (2003) estimated annual net ecosystem production (NEP) using ecological methods. For this comparison, we assumed that NEE = –NEP. The NEE value for the pond surface (P) was obtained from integrated CO_2 emission measurements using the stainless-steel chamber (96 days), on the assumption that photosynthesis and plant respiration could be ignored because of the absence of vascular plants.

2.5.3 Cumulative CH_4 and N_2O fluxes

We calculated the cumulative CH_4 and N_2O fluxes by integrating each day’s measurements.

2.6 Calculation of global warming potential

To evaluate the relative significance of each GHG, we calculated the Global Warming Potential (GWP) as follows (IPCC 2001):

$$\text{GWP (g CO}_2\text{-eq m}^{-2}\text{ period}^{-1}) = \text{NEE (g CO}_2\text{ m}^{-2}\text{ period}^{-1}) + 23 \times \text{CH}_4\text{ emission (g CH}_4\text{ m}^{-2}\text{ period}^{-1}) + 296 \times \text{N}_2\text{O emission (g N}_2\text{O m}^{-2}\text{ period}^{-1}) \quad (5)$$

3. RESULTS

3.1 Soil moisture regime

The seasonal change of soil moisture regime along the line transect is shown in Fig. 2. The volumetric soil moisture content at the soil surface (0 to 6 cm) was lowest from the forest plot to around DG-1 (0 to 40 m from the forest edge) and increased thereafter with increasing proximity to the pond. Soil moisture decreased continuously from the beginning of the measurement period (the end of June) to the end of July. Thereafter, soil moisture increased slightly, reaching a nearly constant value in August and September.

3.2 Seasonal changes in soil temperature, soil moisture, and GHG fluxes

The seasonal changes in soil temperature, soil moisture, soil respiration, CH_4 flux (at the drier sites and wetter sites), and N_2O flux are shown in Fig. 3. In the wet grassland plots (WG-1 and WG-2), CH_4 emissions measured using the transparent chamber were higher than those measured using the stainless-steel chamber under waterlogged conditions, suggesting that CH_4 emission via plants occurred at these sites. Therefore, we used the results from the transparent chamber to represent CH_4 emission from the wet grassland plots.

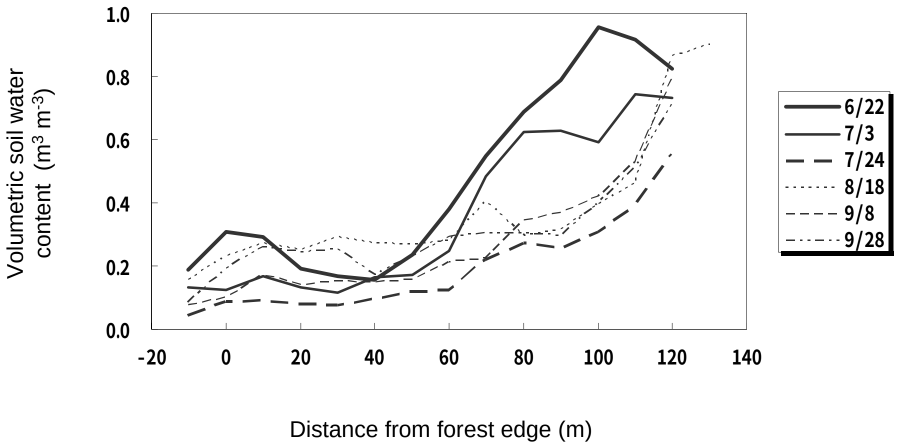

Fig. 2. Seasonal changes in soil moisture content along the transect shown in Fig. 1.

3.2.1 Soil temperature and moisture

Soil temperature at a depth of 3 cm increased from the beginning of the measurement period (early June), when we observed the following temperatures: F, 2.4 °C; DG-1, 6.0 °C; DG-2, 3.3 °C; WG-1, 5.5 °C; and WG-2, 9.2 °C. The maximum values were reached on 9 July: at F, DG-1, DG-2, WG-1, WG-2, and P, these values were 16.6, 22.0, 12.1, 15.4, 21.9, and 28.5 °C, respectively. Thereafter, soil temperatures decreased to near 0 °C at the end of September, when the soil began to freeze.

Soil moisture increased with increasing proximity to the pond, as was shown in Fig. 2. Soil moisture in all plots was highest at the beginning of the measurement period, during the snowmelt, and then decreased continuously from the beginning of the measurement period (the end of June) to the end of July. Thereafter, soil moisture increased slightly then remained nearly constant. The flooding of WG-1 and WG-2 had disappeared by the middle of June and the end of June, respectively, these wet grassland plots dried rapidly.

3.2.2 Soil respiration

Soil respiration showed clear seasonal changes that followed a pattern similar to that of soil temperature, with an increase during the summer and a decrease in autumn. Soil respiration in the grassland plots (31 to 356 mg C m^{-2} hr^{-1}) were generally higher than that in the forest (20 to 150 mg C m^{-2} hr^{-1}) and that measured above the pond surface (22 to 79 mg C m^{-2} hr^{-1}). Soil respiration in WG-1 (wet grassland plot), which was flooded at the beginning of the measurement period, increased rapidly (to a maximum of 356 mg C m^{-2} hr^{-1}) after the flooding disappeared. Thereafter, CO_2 emission remained higher than in the other plots. The cumulative soil respiration values during this measurement period for F, DG-1, DG-2, WG-1, WG-2, and P were 219, 376, 309, 429, 243, and 101 g C m^{-2}, respectively.

3.2.3 CH_4 flux

We found a slight net CH_4 uptake (-12 to 0 µg C m^{-2} hr^{-1}) in the forest plot throughout the measurement period. However, there was no clear seasonal pattern of change. CH_4 fluxes in the dry grassland plots (DG-1 and DG-2) varied between slight net emission and slight net uptake, ranging from -8.8 to 4.9 µg C m^{-2} hr^{-1}. We found remarkably high CH_4 emissions in the wet grasslands (WG-1 and WG-2) and at the pond surface (P) compared to those in the forest and the dry grasslands. In WG-2, CH_4 emissions were highest (39 271 to 40 610 µg C m^{-2} hr^{-1}) during the flooded period in June, but decreased remarkably after the flooding disappeared.

CH_4 emissions from the pond surface, which was continuously flooded, peaked at the beginning of July (3332 to 23 698 μg C m^{-2} hr^{-1}), and then decreased gradually. Cumulative CH_4 emissions during the measurement period for F, DG-1, DG-2, WG-1, WG-2, and P were -0.013, -0.004, -0.010, 1.22, 12.6, and 23.7 g C m^{-2}, respectively.

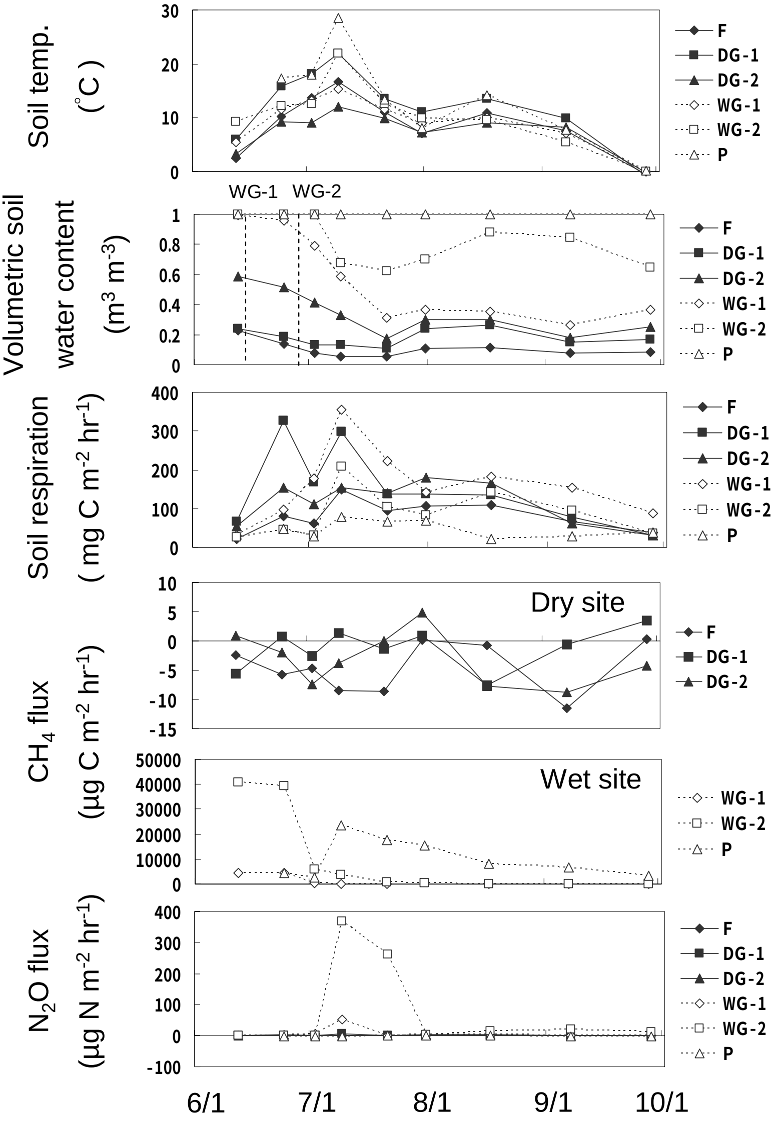

Fig. 3. The seasonal change in soil temperature, moisture, respiration, and CH_4 and N_2O fluxes at the Neleger alas site. A value of 1.0 for the volumetric soil water content represents saturation by pond water. Vertical lines (- - -) in the graph of volumetric soil water content indicate the times when flooding ended in WG-1 and WG-2. For the CH_4 and N_2O fluxes, positive values indicate net emission and negative values indicate net uptake.

3.2.4 N_2O flux

The N_2O fluxes ranged from -0.3 to 1.0 μg N m^{-2} hr^{-1} in the forest plot and -0.5 to 5.0 in dry grassland plots. We observed net N_2O uptake (-2.2 to 0.3 μg N m^{-2} hr^{-1}) at the pond surface almost continuously. During the flooded period, we found no N_2O emission in the wet grassland sites or at the pond surface. However, after the flooding disappeared, we found peak N_2O emission in each wet grassland plot (with a maximum of 368 μg N m^{-2} hr^{-1} in WG-2). Cumulative N_2O emissions during the measurement period for F, DG-1, DG-2, WG-1, WG-2, and P were 0.93, 3.6, 4.8, 16, 173 and -1.7 mg N m^{-2}, respectively.

3.3 CO_2 (NEE)

The relationships between soil temperature and total ecosystem respiration (R_{TOT}) in each grassland plot are shown in Fig. 4 and those between PAR and gross photosynthesis (P_G) in are shown in Fig. 5. Parameters at each site are shown in Table 1. Seasonal changes in the NEE of the grassland plots estimated using the regression equations are shown in Fig. 6. Both CO_2 uptake by photosynthesis and emission by respiration in the wet grassland plots were higher than those in the dry grassland plots (Figs. 4 and 5).

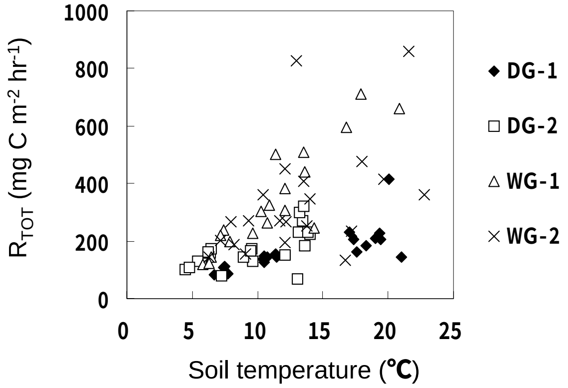

Fig. 4. The relationship between soil temperature at a depth of 3 cm and total ecosystem respiration (R_{TOT}). Significant exponential correlations were found between these parameters at each site (DG-1, $y = 63.08\ e^{0.07x}$, $R^2 = 0.71^{**}$; DG-2, $y = 82.66\ e^{0.07x}$, $R^2 = 0.33^{*}$; WG-1, $y = 81.68\ e^{0.12x}$, $R^2 = 0.79^{**}$; WG-2, $y = 143.58\ e^{0.06\ x}$, $R^2 = 0.26^{*}$).

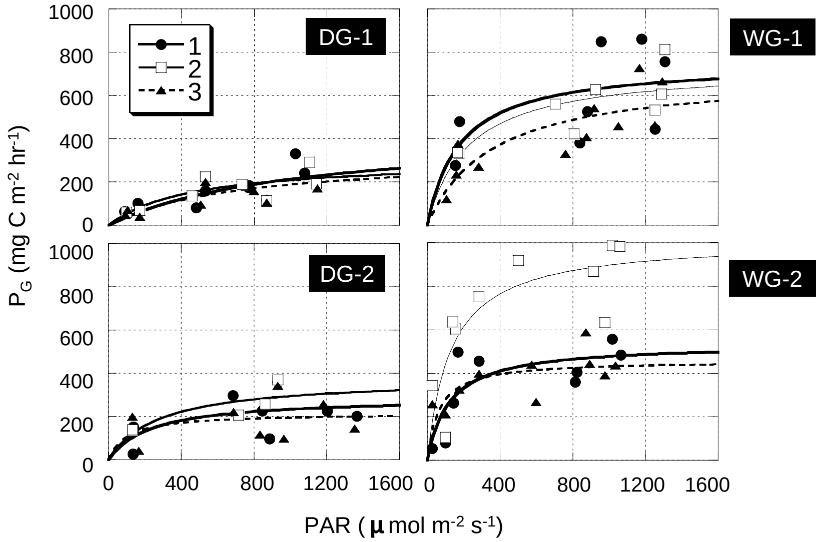

Fig. 5. The relationship between photosynthetically active radiation (PAR) and gross photosynthesis (P_G). The three symbols represent the three replications for each site. Parameters at each site are shown in Table 1.

The cumulative NEE of CO_2 in the dry grassland plots showed net emission throughout the measurement period (DG-1, 204 g C m^{-2} 109 $days^{-1}$; DG-2, 116 g C m^{-2} 109 $days^{-1}$; Fig. 6). In contrast, the WG-1 plot acted as a CO_2 sink during June, when it was flooded by pond water, then became a net source of CO_2 from July to September, after the flooding disappeared. Total CO_2 emission in WG-1 was estimated to be 15.6 g C m^{-2} 109 $days^{-1}$, which was lower than that in the dry grassland plots. The WG-2 plot acted as a CO_2 sink throughout the measurement period (-93.1 g C m^{-2} 109 $days^{-1}$).

The cumulative NEE value for each measurement plot is shown in Fig. 7. CO_2 uptake by the larch forest ecosystem (-140 g C m^{-2} yr^{-1}) was highest among all plots, but the WG-2 plot was also a net CO_2 sink. CO_2 emission from the pond surface (101 g C m^{-2} 96 $days^{-1}$) was slightly lower than that in the dry grassland plots.

Table 1. Parameters for P_G estimating equation in each site.

Site	Rep.	Q	K	n	R^2
DG-1	1	432.3	1027.4	11	0.56 **
	2	304.7	458.9	8	0.59 *
	3	322.8	715.4	10	0.67 **
DG-2	1	288.4	236.1	8	0.36
	2	376.6	279.5	4	0.10
	3	215.2	104.7	8	0.59 *
WG-1	1	752.5	180.44	8	0.34
	2	734.04	225.88	8	0.63 *
	3	701.85	353.42	11	0.64 **
WG-2	1	536.5	123.6	9	0.65 **
	2	1014.3	130.5	10	0.65 **
	3	459.1	64.8	11	0.42 *

*: $p<0.05$; **: $p<0.01$.

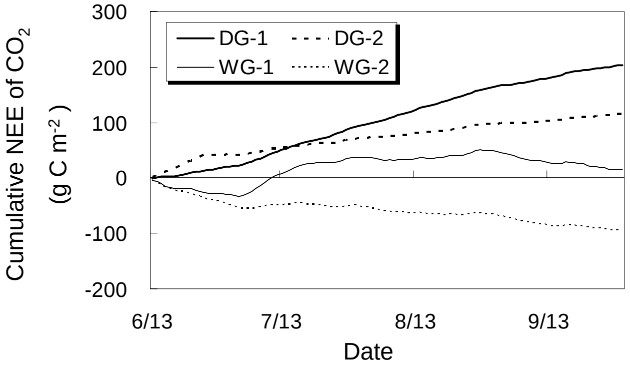

Fig. 6. Cumulative NEE of CO_2. Positive values represent net emission; negative values indicate net uptake.

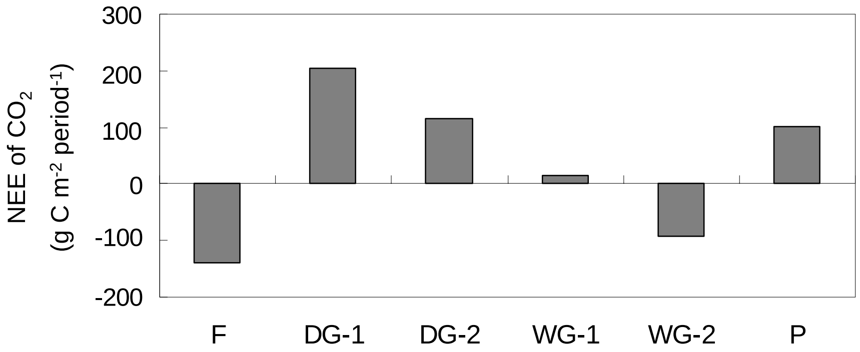

Fig. 7. Cumulative NEE of CO_2 at the Neleger Alas. Emissions from the sites from DG-1 to WG-2 were measured using transparent chambers (with vegetation, 109 days). Emissions from P site were measured using opaque stainless-steel chambers (without vegetation, 96 days). Emissions from the F site were estimated by ecological methods (365 days; Sawamoto et al. 2003).

3.4 GWP

The GWP values for each GHG in each measurement plot are shown in Table 2. Only the forest plot showed a negative value, which suggests that the forest acted as a net sink for GHGs. Most of the GHG uptake by the forest represented CO_2 uptake. On the other hand, the dry grassland plots acted as a net source of GHG, mainly owing to CO_2 emission. The total GWP values in the wet grassland plots were lower than those in the dry grasslands and at the pond surface, but both were also net sources of GHG. In WG-1, CO_2, CH_4, and N_2O were all emitted, and accounted for 56%, 37%, and 7% of the total GWP from this plot, respectively. In WG-2, CO_2 uptake and N_2O emission amounted to 88% and 21% of CH_4 emission, respectively. The total GWP at the pond surface was higher than in any other plot. CO_2 and CH_4 emission accounted for 34% and 66% of the GWP, respectively.

Table 2. The estimated global warming potential (GWP) for each plot.

	Plot	F	DG-1	DG-2	WG-1	WG-2	P
GWP_NEE[a]	$g\ CO_2\text{-eq}\ m^{-2}\ period^{-1}$	-513[c]	747	425	57	-341	369
GWP_CH_4[b]		-0.39	-0.12	-0.30	37	388	728
GWP_N_2O[b]		0.43	1.7	2.2	7.5	81	-0.78
Total	$g\ CO_2\text{-eq}\ m^{-2}\ period^{-1}$	-513	748	427	102	127	1097

[a] Measurement period: 365 days for F, 109 days for DG-1, DG-2, WG-1, and WG-2, and 96 days for P.

[b] Measurement period: 108 days (except for P, for which the period was 96 days)

[c] Sawamoto *et al.* (2003)

4. DISCUSSION

4.1 Soil respiration and NEE

A change in land cover from forest to grassland vegetation could enhance soil respiration (Fig. 3). CO_2 emission from the pond surface was lower than that from the forest floor and the grassland soil surface (Fig. 3). This may have resulted from a decrease in the rate of organic matter decomposition and a suppression of CO_2 diffusion into the atmosphere caused by waterlogged condition. In contrast, CO_2 emissions were lower in the dry grasslands than in the wet grasslands after the flooding disappeared (Fig. 3). This could have resulted from rapid aerobic decomposition of organic matter stored in the waterlogged soils. Consequently, soil moisture conditions, and especially flooding, could be an important factor controlling CO_2 emissions due to the decomposition of organic matter in plots near the pond.

The results of our NEE measurements using the transparent acryl chambers showed that CO_2 emission decreased with increasing proximity to the pond and that CO_2 uptake was possible near the edge of the pond (Figs. 6 and 7). The CO_2 uptake in WG-2 ($-93.1\ g\ C\ m^{-2}\ 109\ days^{-1}$, Figs. 6 and 7) was higher than the values previously reported for flark and lawns in European tundra wetland (-43 to $-17\ g\ C\ m^{-2}\ yr^{-1}$) in north-eastern Europe, Russia (67°N, 63°E; Heikkinen et al. 2002). This suggests that wet alas grassland might be a strong carbon sink. The difference in carbon balance among the grassland plots might have been caused by differences in the photosynthetic ability of the vegetation (Fig. 5) because of the different vegetation present in each plot (Fig. 1), suppression of soil respiration because of flooding (Fig. 3), and other factors. The distribution of grass species in an alas ecosystem might also depend on the water regime. Therefore, soil water regime could exert a strong influence on spatial variation in NEE in an alas grassland. This suggests that it may be possible to estimate NEE based on a parameter such as distance from the pond.

P_G measurements using transparent chamber have possibilities of underestimating for CO_2 uptake by plants because of CO_2 concentration decreasing and air temperature increasing inside the chambers during measurement. More precise inspection for improving chamber measurement is required.

4.2 CH_4 and N_2O fluxes

Net CH_4 uptake occurred in the forest plot. In the alas grassland, CH_4 was taken up or consumed in the relatively drier plots, but was emitted from the wetter plots near the pond (Figs. 3). CH_4 emissions from the plots near the pond were similar to those that have been reported for other wetland ecosystems and paddy fields (Fig. 8). This suggests that the area near the pond in the alas ecosystem is a strong source of CH_4. A rapid decrease in CH_4 emissions after the disappearance of flooded water has been reported from rice paddy fields (Nishimura et al. 2004), suggesting that the CH_4 dynamics of our study area were similar to those of rice paddy fields. CH_4 emission from our study area mainly occurred during flooding. Changes in pond area may control total CH_4 emissions from whole alas ecosystem.

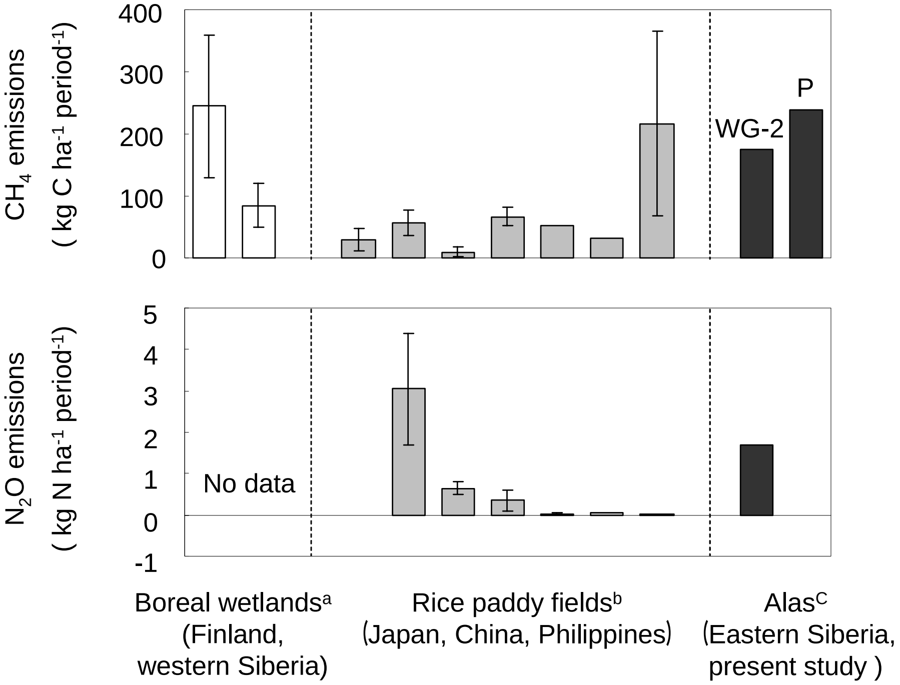

Fig. 8. Cumulative CH_4 and N_2O emissions from natural wetlands, rice paddy fields, and an alas ecosystem (wet grassland (WG-2) and pond surface (P)). Error bars show the range of gas emission.

a) Heikkinen et al. 2002; Alm et al. 1997, annual value. b) Nishimura et al. 2004; Shao and Li et al. 1997, cumulative value for cultivation period. c) The present study, cumulative value for 3 month).

We generally found low N_2O fluxes in all plots, with the exception of wet grasslands during the drying process. In these plots, we found peak N_2O emission after CH_4 emission decreased following the disappearance of flooding (Fig. 3). Similar trade-off relationships between CH_4 and N_2O emissions have been reported from paddy fields after drainage (Nishimura et al. 2004). N_2O emissions could occur in nitrogen-rich paddy fields (e.g., high application of nitrogen fertilizer). To clarify the factors controlling N_2O emission in the alas ecosystem, further studies on soil nitrogen dynamics are required. N_2O emission from our wet alas grassland (WG-2, 1.7 kg N ha^{-1} 108 $days^{-1}$) was a relatively high compared to the values reported from most rice paddy fields (Fig. 8).

4.3 Effect of alas formation on GHG emissions

A severe disturbance of the taiga forest, such as forest fire, can cause the formation of an alas caused by the increased melting of permafrost and the resulting subsidence of the ground (Desyatkin 1993; Isaev 2001). The carbon accumulated in the forest ecosystem is then emitted directly into the atmosphere as CO_2 by the forest fire. On the other hand, our study showed that the wetland ecosystems formed after forest disturbance can potentially accumulate carbon by photosynthesis (Figs. 6 and 7). Schulze et al. (2002) reported that the NEP of a bog ecosystem (43 to 62 g C m^{-2} yr^{-1}) in the middle taiga of Siberia is comparable to that of the surrounding pine forest (60 ± 11 g C m^{-2} yr^{-1}). Although wet grasslands can act as a carbon sink, this fixed carbon might be emitted again as the grasslands dry (Figs. 6 and 7). It is crucial that researchers account for the distribution of each grassland ecosystem when assessing the carbon balance of the overall alas ecosystem.

CO_2 is the only major GHG in the forest ecosystem that does not appear to be affected by alas formation (Fig. 7). On the other hand, CH_4 and N_2O also become important GHGs at the pond and in the nearby grasslands. It is thus also necessary to account for the distribution of each grassland ecosystem and each water regime in an alas ecosystem when assessing the GHG balance of the overall alas ecosystem.

5. CONCLUSIONS

The grassland and pond ecosystems in the Siberian alas in the present study were a net source of GHG. Thus, the grasslands acted as a carbon source. Only sites near the edge of the pond that possessed grassy vegetation were able to sequester carbon. However, this zone around the pond acted as a source of CH_4 and N_2O. The pond itself was a continuous source of CH_4. Our results suggest that when an alas replaces a forest ecosystem, this may change the net GHG balance from a sink to a source and that CO_2, CH_4, and N_2O may all become important GHGs. These GHG balances could be controlled by the soil moisture regime, and especially by flooding due to expansion of the pond water.

Acknowledgments. We are deeply thankful to the staff members of the Institute for Biological Problems of Cryolithozone and the Permafrost Institute, Siberian Branch, Russian Academy of Science for their support during the field research. This study was funded by the CREST program of Japan Science and Technology and by the RR2002 program of the Ministry of Education, Culture, Sports, Science, and Technology of Japan (MEXT).

REFERENCES

Alm J, Talanov AV, Saarnio S, Silvola J, Ikkonen E, Aaltonen H, Nykänen H, Martikainen PJ (1997) Reconstruction of the carbon balance for microsites in a boreal oligotrophic pine fen, Finland.

Oecologia **110**, 423-431.

Aurela M, Laurila T, Tuovinen JP (2004) The timing of snow melt controls the annual CO_2 balance in a subarctic fen. *Geophys. Res. Lett.* **31**, L16119, doi:10.1029/2004GL020315.

Bellisario LM, Bubier JL, Moore TR, Chanton JP (1999) Controls on CH_4 emissions from a northern peatland. *Global Biogeochem. Cycles* **13**, 81-91.

Botch MS, Kobak TS, Vinson TS, Kolchugina TP (1995) Carbon pools and accumulation in peatlands of the former Soviet Union. *Global Biogeochem. Cycles* **9**, 37-46.

Cao M, Gregson K, Marshall S (1998) Global methane emission from wetlands and its sensitivity to climate change. *Atmos. Environ.* **32**, 3293-3299.

Clymo RS (1984) The limits of peat bog growth. *Phil Trans R Soc Lond B* **303**, 605-654.

Desyatkin RV (1993) Syngenetic soil salinization during thermokarst Alas formation. *Eurasian Soil Sci.* **25**, 38-46.

Gorham E (1991) Northern peatlands: Role in the carbon cycle and probable responses to climatic warming. *Ecol. Appl.* **1**, 182-195.

Heikkinen JEP, Elsakov V, Martikainen PJ (2002) Carbon dioxide and methane dynamics and annual carbon balance in tundra wetland in NE Europe, Russia. *Global Biogeochem. Cycles*, **16**, 1115, doi:10.1019/2002GB001930.

IPCC (2001) *Climate Change 2001: The Scientific Basis. Contribution of Working Group I to the Third Assessment Report of the Intergovernmental Panel on Climate Change* [Houghton, J.T.,Y. Ding, D.J. Griggs, M. Noguer, P.J. van der Linden, X. Dai, K. Maskell, and C.A. Johnson (eds)]. Cambridge University Press, Cambridge, United Kingdom and New York, NY, USA, 881pp.

Isaev AP (2001) Post-fire dynamics of larch forests in North-East Siberia (Yakutia). In: Fukuda M, Kobayashi Y (eds) *Proceedings of the ninth symposium on the joint Siberian permafrost studies between Japan and Russia in 2000, 23-24 January 2001, Sapporo, Japan*, pp 3-9. Research Center for North Eurasia and North Pacific Regions, Hokkaido University, Sapporo, Japan.

Kasimir-Klemedtsson A, Klemedtsson L, Berglund K, Martikainen P, Silvola J, Oenema O (1997) Greenhouse gas emissions from farmed organic soils: a review. *Soil Use Manage.* **13**, 245-250.

Kolchugina TP, Vinson TS (1993) Equilibrium analysis of carbon pools and fluxes of forest biomass in the former Soviet Union. *Can. J. For. Res.* **23**, 81-88.

Liblik LK, Moore TR (1997) Methane emissions from wetlands in the zone of discontinuous permafrost: Fort Simpson, Northwest Territories, Canada. *Global Biogeochem. Cycles* **11**, 485-494.

Machimura T, Kobayashi Y, Iwahana G, Hirano T, Lopez L, Fukuda M, Fedorov AN (2005) Change of carbon dioxide budget during three years after deforestation in eastern Siberian larch forest. *J. Agr. Meteorol.* **60** (5), 653-656.

Matthews E, Fung I (1987) Methane emission from natural wetlands: Global distribution, area, and environmental characteristics of sources. *Global Biogeochem. Cycles* **1**, 61-86.

Morishita T, Hatano R, Desyatkin RV (2003) CH_4 flux in an Alas ecosystem formed by forest disturbance near Yakutsk, eastern Siberia, Russia. *Soil Sci. Plant Nutr.* **49**, 369-377.

Nishimura S, Sawamoto T, Akiyama H, Sudo S, Yagi K (2004) Methane and nitrous oxide emissions from a paddy field with Japanese conventional water management and fertilizer application. *Global Biogeochem. Cycles* **18**, GB2017, doi:10.1029/2003GB002207.

Regina K, Nykänen H, Silvola J, Martikainen PJ (1996) Fluxes of nitrous oxide from boreal peatlands as affected by peatland type, water table level and nitrification capacity. *Biogeochemistry* **35**, 401-418.

Sawamoto T, Hatano R, Shibuya M, Takahashi K, Isaev AP, Desyatkin RV, Maximov TC (2003) Changes in net ecosystem production associated with forest fire in Taiga ecosystems, near Yakutsk, Russia. *Soil Sci. Plant Nutr.* **49**, 493-501.

Schulze ED, Prokuschkin A, Arneth A, Knorre N, Vaganov EA (2002) Net ecosystem productivity and peat accumulation in a Siberian Aapa mire. *Tellus* **54B**, 531-536.

Shao K, Li Z (1997) Effect of rice cultivars and fertilizer management on methane emission in a rice paddy in Beijing. *Nutr. Cycl. Agroecosyst.* **49**, 139–146.

Shurpali NJ, Verma SB, Clement RJ, Billesbach DP (1993) Seasonal distribution of methane flux in a Minnesota peatland measured by eddy correlation. *J. Geophys. Res.* **98** (D11), 20649-20655.

Takahashi K, Isaev AP, Maximov TC, Saito H (2003) Fire history of mature larch forests near Yakutsk Eastern Siberia. In: Fukuda M, Saito H (eds) *Proceedings of the 10th symposium on the joint Siberian permafrost studies between Japan and Russia in 2001, 22-23 March 2002, Tsukuba, Japan*, pp 65-68. Research Center for North Eurasia and North Pacific Regions, Hokkaido University, Sapporo, Japan.

Turunen J, Tomppo E, Tolonen K, Reinikainen A (2002) Estimating carbon accumulation rates of undrained mires in Finland – application to boreal and subarctic regions. *The Holocene* **12**, 69-80.

Waddington JM, Roulet NT (2000) Carbon balance of a boreal patterned peatland. *Global Change Biol.* **6**, 87-97.